Volume 6 Issue 1 (March 2026)
DOI 10.24191/jaeds.v6i1.177
eISSN 2805-5756

Journal of Applied Engineering Design & Simulation

Numerical Investigation of Coupled Intralaminar and Interlaminar Damage In Toughened CFRP Laminates Subjected to Low-Velocity Impact

M.H.A Ismail[1], R. Othman[1*] and M.R. Aziz[1]
[1]Mechanical Engineering Studies, Universiti Teknologi MARA Cawangan Pulau Pinang, 13500 Permatang Pauh, Penang, Malaysia.
[*]corresponding author: rozaini.othman@uitm.edu.my

ABSTRACT

Carbon fibre reinforced polymer (CFRP) laminates are widely used in lightweight structural applications because of their excellent strength-to-weight ratio. Despite these advantages, CFRP structures are particularly susceptible to barely visible damage when subjected to low-velocity impact. Such damage often results from complex interactions between intralaminar matrix cracking and interlaminar delamination, a problem that becomes more pronounced in laminates incorporating particle-toughened interlayers. Although many numerical studies have examined impact damage in composite materials, most existing models focus on conventional laminates and do not adequately represent the coupled intralaminar–interlaminar damage behaviour associated with toughened interlayers. In this study, a numerical framework is developed to examine the progressive damage behaviour of CFRP laminates with toughened interlayers under low-velocity impact loading. A finite element model is implemented in ABAQUS/Explicit, combining Hashin's intralaminar failure criteria with cohesive zone modelling to simulate both interlaminar delamination and intralaminar damage. The impact responses of unidirectional and cross-ply laminates are investigated using spherical, conical, and flat impactors with identical mass and material properties. Model validation is carried out by comparing displacement–time responses with published numerical data, showing good agreement. The results demonstrate that both laminate configuration and impactor geometry play a significant role in governing deformation, stress distribution, and damage development. Cross-ply laminates exhibit higher stress concentrations due to ply orientation mismatch, whereas unidirectional laminates show better load-carrying capability. Matrix-dominated damage, particularly compressive matrix failure, is identified as the dominant failure mode across all impact conditions. In addition, flat and spherical impactors produce greater displacement and more severe damage than conical impactors as a result of their larger contact areas. Overall, the proposed framework provides clearer insight into the coupled damage mechanisms of toughened CFRP laminates and offers practical guidance for designing impact-resistant composite structures in aerospace and automotive applications.

Keywords: CFRP toughened interlayer; low-velocity impact; interlaminar delamination; intralaminar damage; finite element analysis.

Nomenclature

σ	stress matrix (MPa)
C	stiffness matrix (MPa)
ε	strain matrix (m/m)
F_f^t	internal thermal resistance of the TEG (Ω)
σ_{11}	normal stress in the fibre direction (MPa)
σ_{22}	normal stress in the transverse direction (MPa)
τ_{12}	shear stress in the plane of fibre and transverse directions (MPa)
X^T	tensile strength in the fibre direction (MPa)
X^C	compressive strength in the fibre direction (MPa)
Y^T	tensile strength in the transverse direction (MPa)
Y^C	compressive strength in the transverse direction (MPa)
S^L	shear strength in longitudal direction (MPa)
S^T	shear strength in transverse direction (MPa)
σ_n	stress in normal (MPa)
σ_s	shear stress (MPa)
σ_t	shear stress (MPa)
G_{shear}	rate of energy release for mixed-mode shear loading
G_T	the total energy release rate

Received on 01.03.2026
Accepted on 23.04.2026
Published on 06.05.2026

Abbreviations

CFRP	carbon fibre reinforced plastics

1.0 INTRODUCTION

The applications of composite materials have grown tremendously due to the favorable properties that it possessed. The great porperties characteristic, such as high-specific strength, stiffness and modulus, as well as good fatigue properties, have made composite materials so desirable in the area of aerospace, marine, automotive, and defense industries [1]. Despite these advantages, laminated composites exhibit weak through-thickness properties, making them vulnerable to impact-induced delamination [2]. Low-velocity impact typically generates internal matrix cracking and fibre fracture without obvious surface damage, commonly referred to as BVID [3].

Delamination significantly reduces residual compressive strength and structural integrity [4]. Numerical modelling has therefore become a critical tool for predicting damage behaviour. Hashin's failure criteria are widely adopted for intralaminar failure prediction [5], while cohesive zone modelling has proven effective for simulating interlaminar delamination [6]. To improve the interlaminar fracture toughness, an interlayer is often introduced by replacing the resin at prepreg surface to a tougher system such as the inclusion of thermoplastic particle. Figure 1 depicts CFRP toughened with interlayer prepreg. According to Lee et al. [5], by adding the tough adhesive layer, fracture toughness of modes I and II are able to be increased. At present, the numerical model is only limited on interlaminar delamination and intralaminar damage of CFRP laminate without considering toughened interlayer.

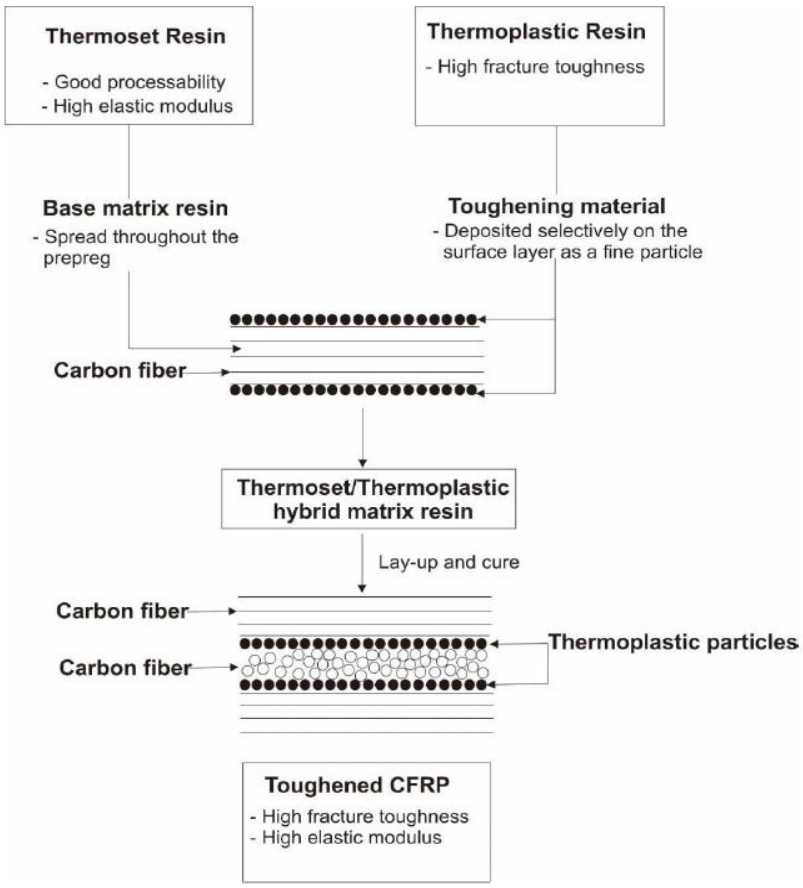

Figure 1. CFRP toughened with interlayer prepreg. Reproduced based on Odagiri et al. [7]

Recent studies have investigated toughened interlayers to enhance fracture toughness under mixed-mode loading conditions [8,9]. This study aims to develop an integrated numerical framework to capture the coupled interaction between intralaminar and interlaminar damage.

2.0 METHODOLOGY

2.1 Introduction

Finite element analysis simulation of the low-velocity impact test was conducted by using ABAQUS /Explicit software. The constitutive modelling of CFRP and the interlayer is described first. Following that, the base ply failure criterion and delamination modelling are explained. Figure 2 depicts the overall modelling process in ABAQUS/Explicit.

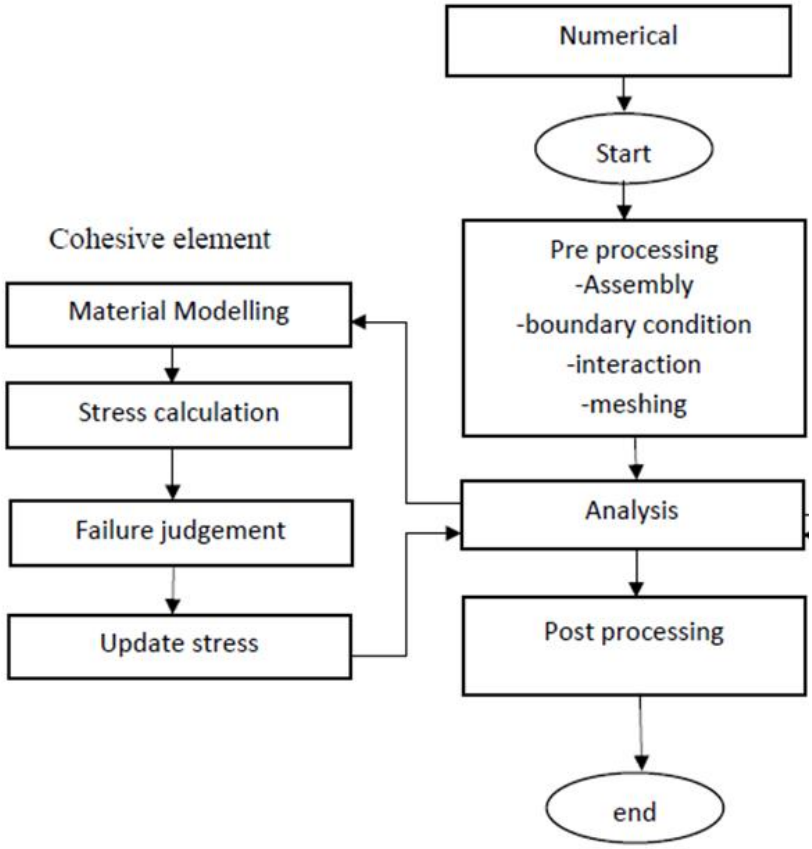

Figure 2. Flow chart of ABAQUS/Explicit numerical simulation.

2.2 Constitutive modelling

The base plies were considered to be orthotropic elastic bodies, whereas the interlayers were modelled as isotropic perfect elasto-plastic bodies. A similar strategy was utilised by Shigemori [10], who proposed that a laminate would consist of two layers: a base-ply and an interlayer. Composite materials are anisotropic by nature, hence their stress-strain relationship has 21 separate constants. The expression of stress-strain is shown in Equation (1). For the interlayer, it was considered to be isotropic. The base-ply and the interlayer properties were accumulated in Table 1 and 2.

$$\sigma = C\varepsilon \quad (1)$$

Table 1: Base-ply and interlayer properties [10]

Property	Base Ply		Interlayer
Young's modulus *E* (GPa)	Longitunal E_1	151	4.6
	Transverse E_2	9.16	
Shear modulus *G* (GPa)	$G_{12} = G_{13}$	4.62	1.6
	G_{23}	2.55	
Poisson's ratio *v*	$\nu_{12} = \nu_{13}$	0.302	0.44
	ν_{23}	0.589	
Yield Strength (MPa)			64

Table 2: Base-ply strength properties [10]

Direction of strength	Strength (MPa)
Tensile strength in the fibre direction	3108
Compressive strength in the fibre direction	719.4
Tensile strength in the transverse direction	67
In-plane shear strength	100
Out-of-plane shear strength	100

2.3 Damage criteria

Both fibre and matrix damage were considered for the damage criteria. The normal stress in the fibre direction leads to the fibre damage, while the normal stress in transverse direction and the shear stress in the plane of fibre and transverse directions contributed to the matrix damage. Hashin damage criteria was used to model the damage appeared within layers. The criteria were formulated as follows:

Fibre damage:

$$\mathrm{F_f^t} \equiv \left(\frac{\sigma_{11}}{\mathrm{X^T}}\right)^2 + \alpha\left(\frac{\tau_{12}}{S^L}\right)^2 \geq 1 \ , (\sigma_{11} \geq 0) \tag{2}$$

$$\mathrm{F_f^c} \equiv \left(\frac{\sigma_{11}}{\mathrm{X^C}}\right)^2 \geq 1 \ , (\sigma_{11} < 0) \tag{3}$$

Matrix damage:

$$\mathrm{F_m^t} \equiv \left(\frac{\sigma_{22}}{\mathrm{Y^T}}\right)^2 + \left(\frac{\sigma_{12}}{S^L}\right)^2 \geq 1 \ , (\sigma_{22} \geq 0) \tag{4}$$

$$\mathrm{F_m^C} \equiv \left(\frac{\sigma_{22}}{2S^T}\right)^2 + \left[\left(\frac{\mathrm{Y^C}}{2S^T}\right)^2 - 1\right]\left(\frac{\sigma_{22}}{Y^C}\right) + \left(\frac{\tau_{12}}{S^L}\right)^2 \geq 1 \ , (\sigma_{22} < 0) \tag{5}$$

2.4 Delamination modelling

The modelling of delamination was carried out based on the work done by Camanho and Davilla [11,12] and it was implemented using the ABAQUS/Explicit software. Interface elements were inserted between plies of the modelling, in which the elements were denoted as cohesive elements. The analysis of delamination in composite laminate was carried out in two phases: the first stage was the initiation of delamination, and the second phase was the propagation of delamination.

2.4.1 Damage initiation

The delamination initiation was predicted based on a quadratic equation law, which assumes that the damage initiation begins when the quadratic interaction function equals to one. The quadratic equation based on stresses is expressed in Equation (6) [13]

$$\left(\frac{\langle\sigma_n\rangle}{N}\right)^2 + \left(\frac{\sigma_s}{S}\right)^2 + \left(\frac{\sigma_t}{T}\right)^2 = 1 \tag{6}$$

2.4.2 Damage evolution

The failure criterion used to compute propagation of delamination was based on energy release rates under mixed mode loading; modes I, II, and III. The progression of damage was due to the energy dissipated by the damage process, commonly known as the fracture energy. The Benzeggagh-Kenane fracture criterion was applied in which the fracture energy that occurred during deformation primarily along the first and second shear directions was identical [14]. For a mixed mode fracture, the damage increased when the energy release rate was equal to or greater than the critical energy release rate, G^C. The cohesive element properties used to simulate delamination are presented in Table 3, as extracted from the work of Morimoto [15] and Hojo [16]. The η parameters were obtained from the work of Ogi [17].

$$G^C = G_{IC} + (G_{IIC} - G_{IC}) \left\{ \frac{G_{shear}}{G_T} \right\}^{\eta} \quad (7)$$

Table 3: Properties of cohesive elements.

Properties	Interlaminar delamination [15]	Intralaminar damage [16]
In-plane tensile strength t_n N (MPa)	80	60
In-plane and out of plane shear strength t_s, t_t (MPa)	160	100
Mode I critical energy release rate, G_{IC} (J/ m^2)	540	200
Modes II & III critical energy release rate, G_{IIC} & G_{IIIC} (J/m^2)	1640	500
η parameter [17]	1.5	1.5

2.5 Finite Element Model

Due to the symmetrical of the laminates, a quarter model was decided to be produced with the total thickness of 3 mm and 36 plies in which the interlayer was inserted for each ply. The thickness of each base-ply 0.375 mm and the thickness of the interlayer was 0.04 mm. The thickness is proportionate with published study [8]. Both base-plies and interlayers were employed with shell elements (SC8R) as shown in Figure 3. The stacking sequences of the models were unidirectional lamination $[0°]_{36}$ and cross-ply lamination $[0°/90°]_{18S}$. The impactor was assumed to be a rigid body with a spherical head and a diameter of 6 mm and a mass of 500 g. To further investigate, two other types of impactors were also selected, namely cone and flat impactor. The projectile's initial velocity was applied to simulate the impact event. The pre-determined velocity of impact was 2-8 m/s. Furthermore, cohesive elements were incorporated to represent delamination generated between the base ply and the interlayer as well as inside the base plies, as seen in Figure 4. The delamination between plies was entitled as interlayer delamination and the damage within plies was entitled as intralayer damage. The mesh elements of the laminates were created based on finite element techniques of Eularian analysis adopted by ABAQUS/Explicit software.

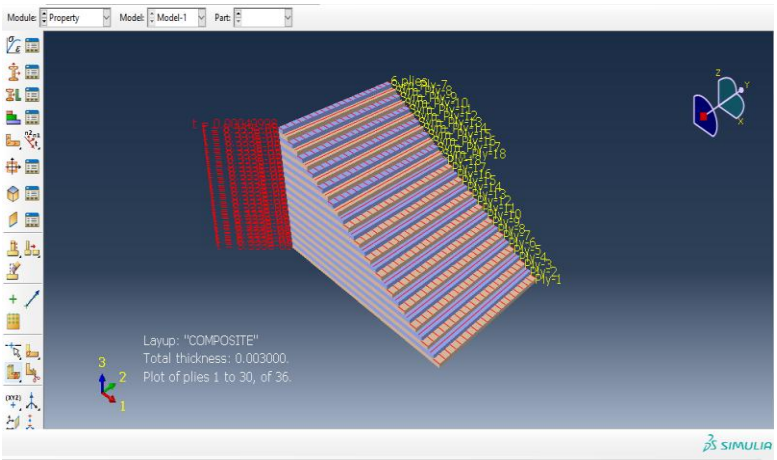

Figure 3. The ply sequence of composite plate.

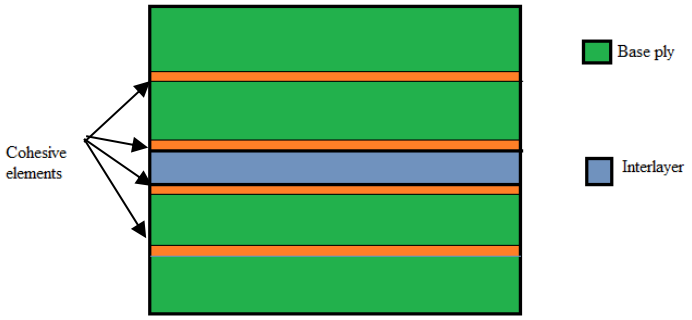

Figure 4. Cohesive elements insertion in the FEA model at the interfaces of interlayer with base ply and within base ply.

To differentiate between interlaminar delamination and intralaminar damage behaviour, the simulation was done separately. Meanwhile, for the interlaminar delamination, the cohesive elements were only introduced between the plies. For both interlaminar delamination and intralaminar damage, the cohesive elements were introduced between the plies and within the plies.

2.5.1Interaction and contact modelling

The contact modelling was analysed by utilizing general contact algorithm in ABAQUS/Explicit. The contact comprised contact between impactor and the laminate and internally adjacent plies of the laminate. This contact algorithm has fewer restrictions that enable the modelling of element erosion using an element-based surface, which may be used while the study was being carried out. Additionally, the general contact algorithm generated a contact force based on the penalty enforcement contact approach. The coefficient of friction was utilised to account for the shear stress of surface traction with contact pressure.

In general, the friction coefficient was determined by the material's stiffness and the surface's roughness. Previous research suggested using 0.2 as the coefficient of friction for 0°/0° laminates and 0.8 for the contact between adjacent 90° and 45° plies [46]. In previous study, a mean coefficient of friction of 0.5 was used between the 0°/90° interface of cross-ply laminate [17]. The tie constraint method was another method for modelling contacts. The objective of this contact approach is to connect the surface of a cohesive element to the surface of a solid element to provide continuity between these two types of elements. In this approach, the solid element was considered the master surface and the cohesive element was considered the slave surface.

2.5.2 Boundary conditions

The laminate has its edges clamped in order to simulate the conditions of based on the published experiment. Therefore, the modelling of the laminate was done with the edges of the laminate being fixed along all three axes ($x = 0$, $y = 0$, and $z = 0$). At the cross section of the laminate, symmetrical boundary conditions along the x and y axes were applied because the laminate was modelled as a quarter.

In addition, a tie constraint was added between the laminate's cohesive parts and its solid elements. On the other hand, the impactor was fixed along the x and y axes, but it was enabled for movement along the z axis. Due to the fact that the impactor was modelled as a rigid body, the reference point was positioned at the nose of the impactor, and the value of the velocity along the z axis was established at the reference point.

2.6 Projectile

In this study, three different projectile geometries namely spherical, conical, and flat were employed to investigate how CFRP laminates respond to varying impactor shapes. Using different rigid body profiles allow the assessment of how projectile geometry influences impact behaviour and damage progression within the composite. All projectiles were assigned identical parameters, including a diameter of 6 mm and a mass of 500 g. The density was set to 7800 kg/m³, corresponding to the 304 stainless steel material used. Each projectile was modelled as deformable, following the methodology adopted in the referenced literature. The mechanical properties were defined as isotropic, with a Young's modulus of 200 GPa and a Poisson's ratio of 0.3.

3.0 RESULTS AND DISCUSSION

3.1 Numerical validation at impact velocity of 5 m/s

The validation of the model was made by comparing the maximum displacement obtained in ABAQUS/Explicit with the published results [8]. Similar pattern was observed when impacted with a composite plate at impact energy of 50 J and 100 J. The displacement of the composite laminate at low velocity of 5 m/s

obtained from ABAQUS/Explicit was depicted by displacement-time graph in Figure 5. The maximum displacement of 4.3 mm occurred at the impact region of the laminate particularly at node 15. After the impact took place (0-0.2 ms), a slight displacement occurred on the laminate. Gradual increase in displacement was observed after 0.2 ms up to a maximum displacement of 4.3 mm. The maximum displacement occurred at 1.1 ms after the impact event. The displacement of the laminate started to reduce slowly, and it indicated that the impactor began to rebound. The deformation contour of CFRP cross-ply laminate at the impact velocity of 5 m/s is depicted in Figure 6. All figures show similar deformation pattern when the impactor hit the laminate.

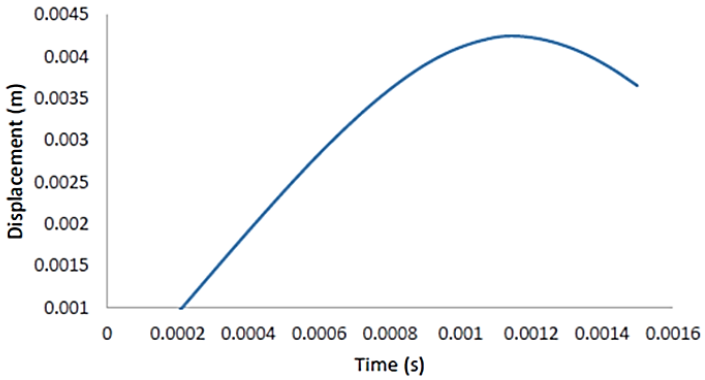

Figure 5. The graph of displacement against time at velocity of 5 m/s for a cross-ply laminate

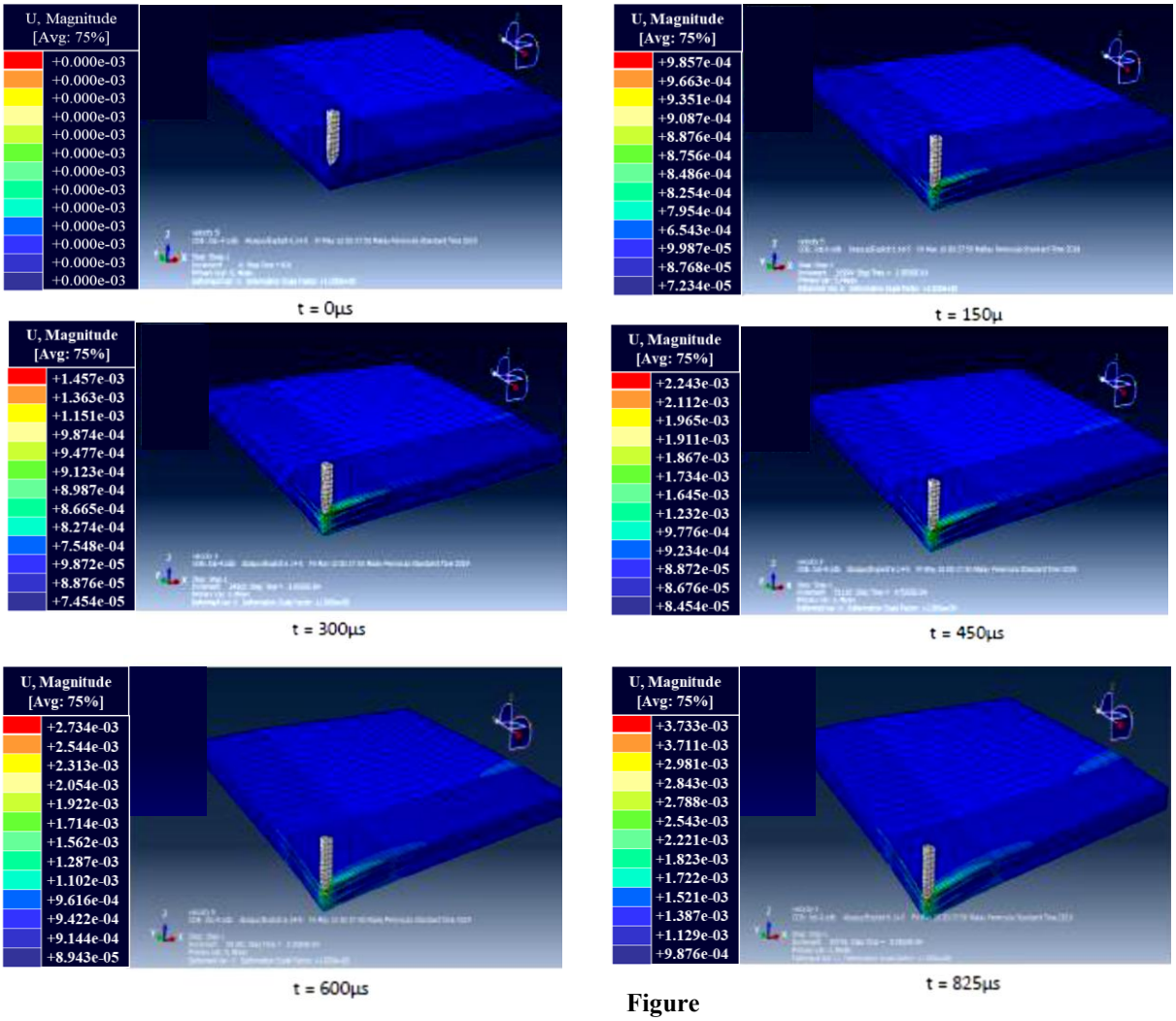

Figure

Figure 6. The deformation contour of cross-ply laminate when impacted at velocity of 5 m/s.

The displacement of unidirectional CFRP laminate at velocity of 5 m/s is depicted by displacement-time graph in Figure 7. At impact velocity of 5 m/s, a slight displacement occurred at the beginning as the impactor started to hit the laminate. After that, the displacement at impact point was almost linear up to t = 1 ms. The maximum displacement was 3 mm at t = 1.1 ms. The deformation contour of the unidirectional CFRP laminate for impact velocity of 5 m/s is depicted in Figure 8. All figures show similar deformation pattern as the impactor hit the laminate.

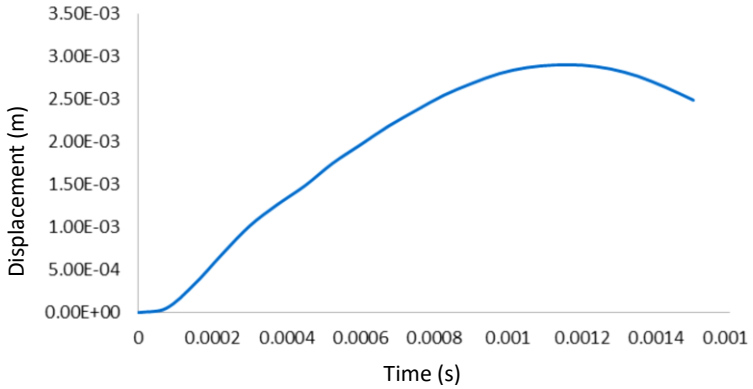

Figure 7. The graph of displacement against time at velocity of 5 m/s for a unidirectional laminate.

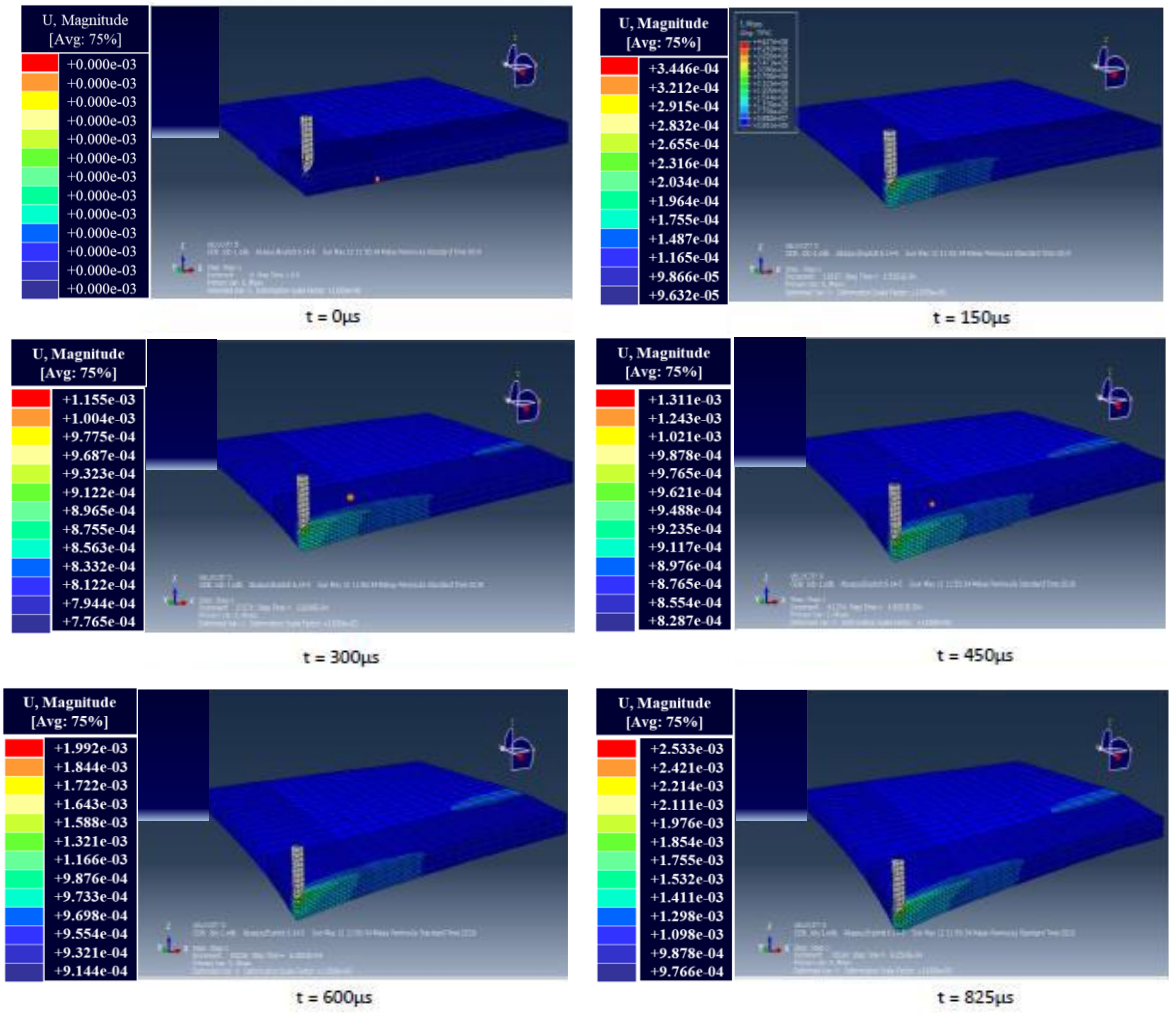

Figure 8. The deformation contour of unidirectional laminate when impacted at velocity of 5 m/s.

Stress distribution of the laminate after the impact event is depicted in Figure 9 and Figure 10 respectively. The cross-ply laminate exerted higher stress compared to unidirectional laminate. It could possibly be due to stress propagated in both fibre and transverse directions and thus, lead to higher stress. On the other hand, unidirectional laminate can sustain large amount of load compared to cross-ply laminate.

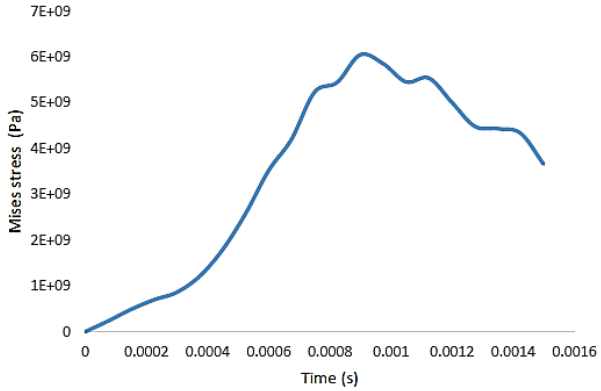

Figure 9. Stress distribution for cross-ply laminate at impact velocity of 5 m/s.

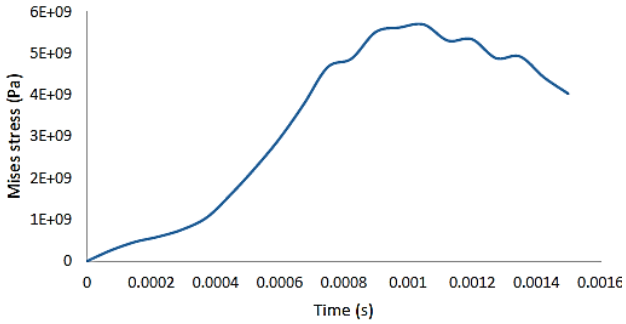

Figure 10. Stress distribution for unidirectional laminate at impact velocity of 5 m/s.

3.2 Deformation with different types of impactor

The different types of impactors also contribute to the different behaviour of damage. In deformation analysis of CFRP plate, the displacement results were extracted from the simulation to determine the extent of deformation experienced by the composite material when impacted by projectiles at 5 m/s. As this study focused on low-velocity impact, the resulting displacement values were relatively small. The spatial displacement data are presented in the bar chart shown in Figure 11. Based on Figure 11, composite plate hit by flat and spherical projectile recorded the highest value of spatial displacement followed by composite plate hit by cone shape projectile. It can be concluded that composite plate hit by projectile that has bigger surface leads to bigger value of spatial displacement.

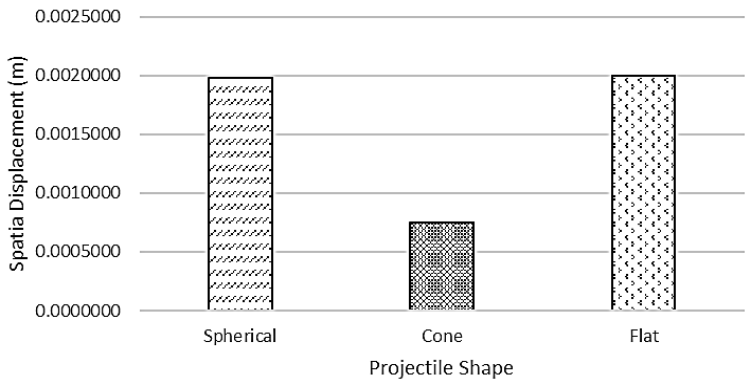

Figure 11. Spatial displacement value at 5 m/s

3.3 Damage of CFRP toughened interlayers due to impact

Both fibre and matrix damage were incorporated into the damage evaluation criteria. Fibre damage is primarily governed by normal stresses acting along the fibre direction, whereas matrix damage is influenced by normal stresses in the transverse direction as well as shear stresses within the fibre–transverse plane. The Hashin damage criteria were applied to model the initiation and progression of damage within each composite layer [18]. The criteria include:

i. Hashin compressive fibre initiation criterion.
ii. Hashin tensile fibre initiation criterion.
iii. Hashin compressive matrix initiation criterion.
iv. Hashin tensile matrix initiation criterion.

Matrix cracking and delamination are the primary damage mechanisms associated with low-velocity impacts. In the aviation industry, low-velocity impact typically refers to impact energies of 5 J or less, often resulting from dropped tools or small debris striking the aircraft during manufacturing or maintenance processes [19]. Accordingly, the impact velocities in this study were selected based on kinetic energy values below 5 J. Using the kinetic energy equation, the corresponding impact velocities were calculated to be 4.5 m/s.

3.3.1 Hashin's compressive fibre initiation criterion

Figure 12 indicates the element failure pattern of the composite plate at a velocity of 4.5 m/s. Element failure occurred in the composite plate impacted by the spherical and conical projectiles.

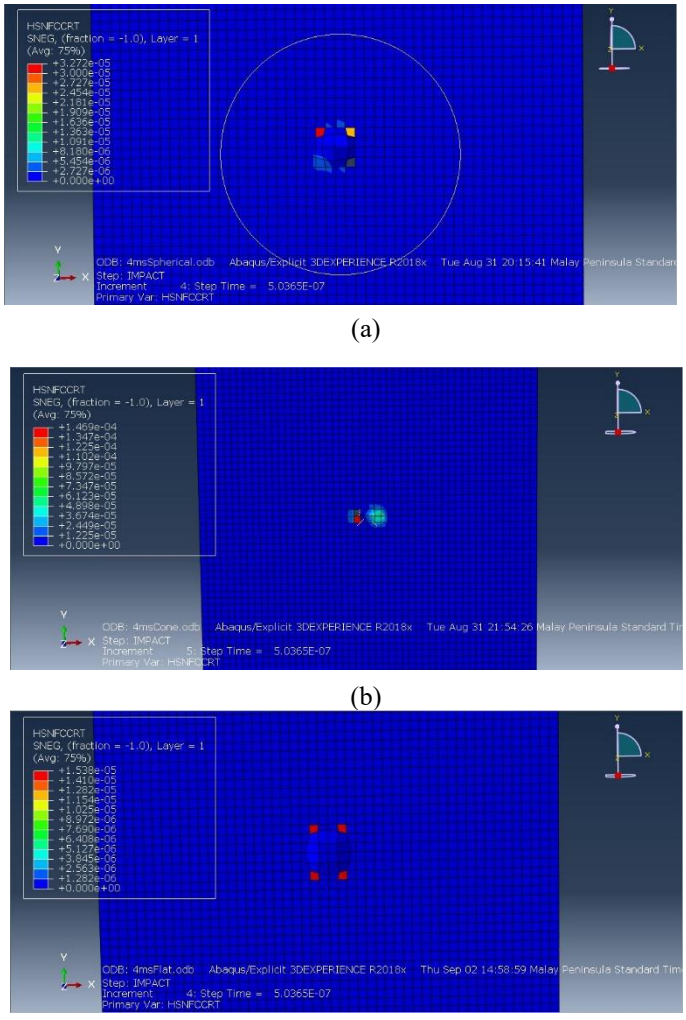

Figure 12. Deformation of Hashin's compressive fibre at 4.5m/s velocity: (a) spherical projectile; (b) cone projectile; (c) flat projectile.

3.3.2 Hashin's tensile fibre initiation criterion

Figure 13 shows that the composite plates impacted by the spherical and flat projectiles at a velocity of 4.5 m/s exhibited element failure, whereas the plate impacted by the conical projectile did not. This indicates that the spherical and flat impactor geometries generate higher localized stresses or more severe contact interactions at this velocity, leading to damage initiation within the laminate.

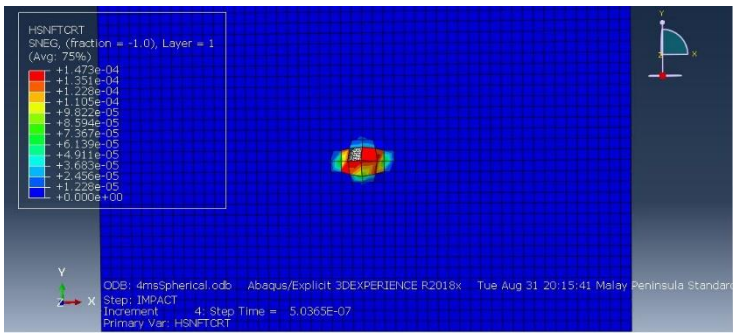

(a)

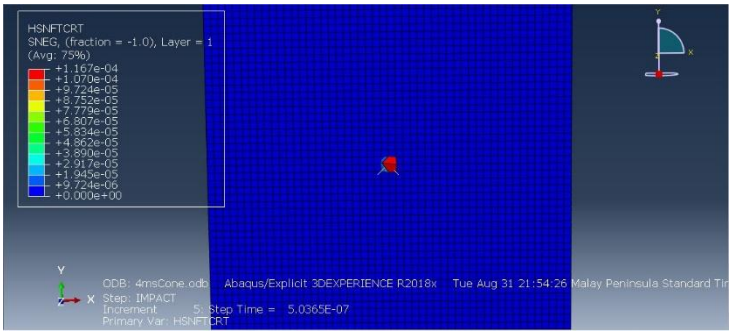

(b)

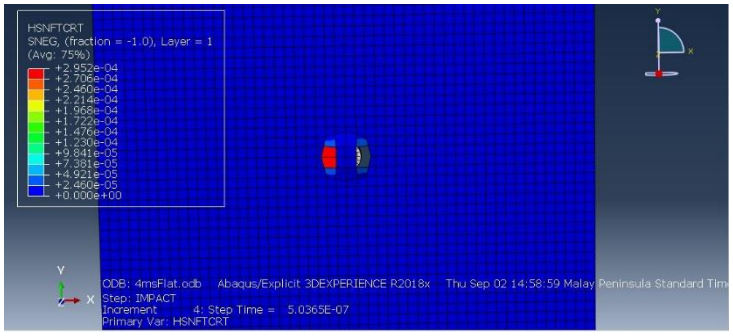

(c)

Figure 13. Deformation of Hashin's tensile fibre at 4.5 m/s velocity: (a) spherical projectile; (b) cone projectile; (c) flat projectile.

3.3.3 Hashin's compressive matrix initiation criterion

Based on Figure 14, among the three composite plates, only the specimen impacted by the flat-surface projectile exhibited element failure. This indicates that the flat impactor generates a stress distribution that is more severe or more concentrated within the laminate compared to the spherical and conical projectiles under the same impact conditions.

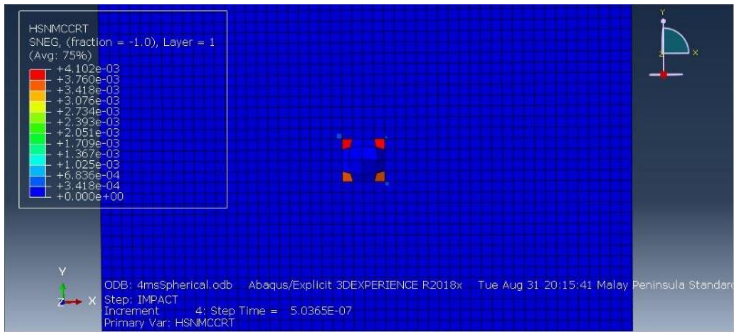

(a)

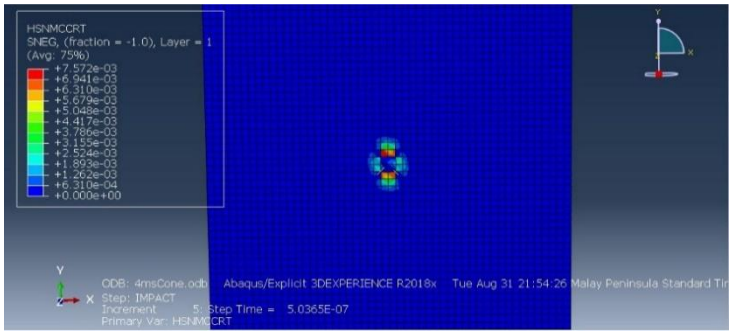

(b)

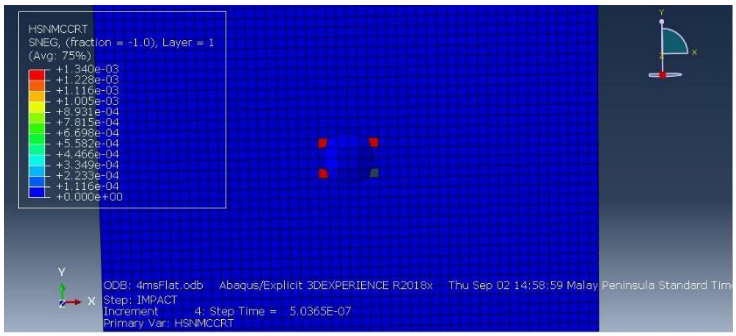

(c)

Figure 14. Deformation of Hashin's compressive matrix at 4.5 m/s velocity: (a) spherical projectile; (b) cone projectile; (c) flat projectile.

3.3.4 Hashin's tensile matrix initiation criterion

Figure 15 depicts the deformation of Hashin's tensile matrix at 4.5 m/s velocity. When the three composite plates were impacted at a velocity of 4.5m/s by the spherical, conical, and flat projectiles, none of them exhibited element failure according to Hashin's tensile matrix damage criterion. Although the impact energy at this velocity was higher than in the previous cases, the tensile stresses generated within the matrix remain below the critical threshold required to initiate damage. This suggests that the laminate structure possesses sufficient tensile resistance in the matrix phase to withstand the applied loading conditions.

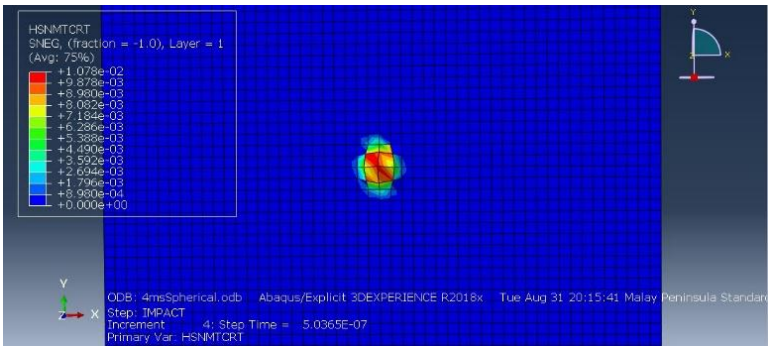

(a)

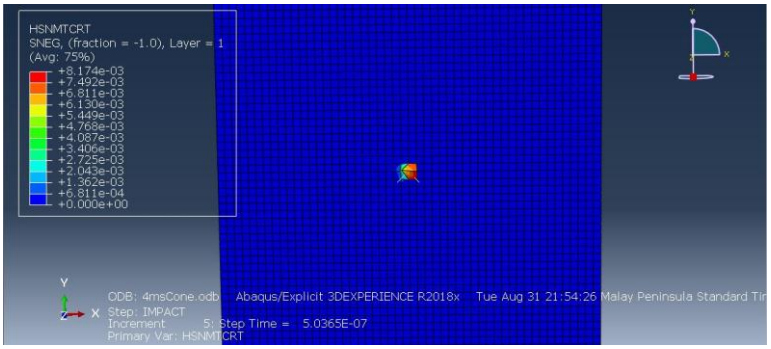

(b)

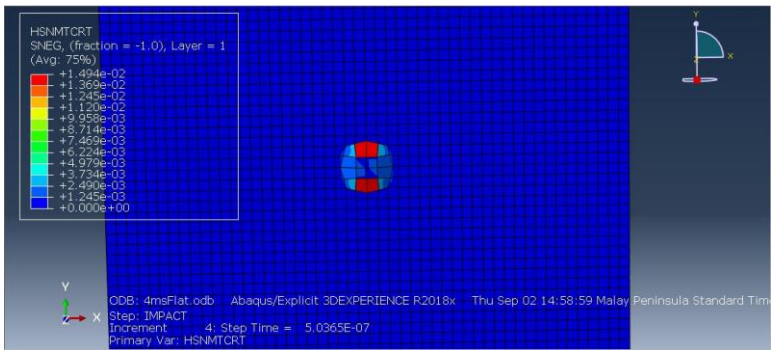

(c)

Figure 15. Deformation of Hashin's tensile matrix at 4.5m/s velocity: (a) spherical projectile; (b) cone projectile; (c) flat projectile.

3.4 Discussion

The numerical validation performed at impact velocities of 5 m/s demonstrates that the simulated displacement responses closely follow the trends reported in the literature, confirming the reliability of the ABAQUS/Explicit model used in this study. At 5 m/s, the composite laminate exhibited a maximum displacement of 4.3 mm at approximately 1.1 ms, after which rebound behaviour was observed. These responses are consistent with typical low-velocity impact characteristics of composite laminates, where deformation increases proportionally with impact energy until the onset of rebound, as also reported in previous studies [8]. This agreement verifies the fidelity of the model and supports its use in subsequent parametric impact analyses.

Comparison between cross-ply and unidirectional laminates reveals clear structural differences in their impact responses. Cross-ply laminates experience higher overall stress levels due to load transfer occurring in both fibre and transverse directions, whereas unidirectional laminates demonstrate the ability to sustain greater loads with lower stress concentrations. The displacement-time curves further confirm that unidirectional laminates maintain a more stable deformation pattern under increasing velocity, aligning with established findings that fibre-dominated directions in CFRP composites offer superior load-bearing capacity [20]. These structural distinctions highlight the importance of laminate orientation in designing components subjected to low-velocity impacts.

The results also show that projectile geometry has a significant influence on deformation behaviour at low-velocity conditions. At 5 m/s, flat and spherical projectiles produced the highest spatial displacement compared to the conical projectile. This is likely due to the larger contact area of the spherical and flat impactors, which promotes broader distribution of impact loads and consequently greater out-of-plane deformation. Previous studies similarly indicate that impactors with larger surface areas transfer greater energy into bending deformation rather than initiating immediate localized damage [21]. Hence, the findings support the conclusion that impactor shape is a critical parameter in predicting displacement and potential damage progression of composite structures.

Analysis using Hashin's failure criteria reveals distinct differences between fibre-dominated and matrix-dominated failure mechanisms under varying impact velocities. Fibre compression and tension failures occur selectively depending on projectile geometry, with spherical projectiles often producing more concentrated stresses that trigger earlier fibre damage. Meanwhile, matrix damage for both compressive and tensile are generated more consistently across all velocities, indicating that the matrix phase is more susceptible to failure under low-velocity impact loading. This aligns with established literature that stated matrix cracking and delamination are the predominant damage modes in low-energy impacts [18], particularly because matrix-dominated zones absorb less energy before failure compared to the fibre-dominated regions [19]. These results underscore the sensitivity of matrix behaviour in governing the overall structural response.

The combined effect of laminate orientation, projectile geometry, and impact energy produced clear and predictable damage patterns. Importantly, tensile matrix failure was not triggered at 4.5 m/s, suggesting that the laminate possesses sufficient tensile resilience to resist crack propagation under these specific conditions. Overall, these trends reinforce the necessity of understanding both material behaviour and impact geometry when designing CFRP components for safety-critical applications.

4.0 CONCLUSION

A few conclusions can be made from the study of intralaminar and interlaminar damage behaviour of carbon fibre reinforced plastics (CFRP) with toughened interlayers subjected to impact loading.

The numerical model developed using ABAQUS/Explicit successfully replicated the displacement trends reported in previous experimental and numerical studies. There is close agreement of maximum displacement and rebound behaviour at impact velocities of 5 m/s.

The results clearly demonstrate that laminate orientation significantly affects the deformation and stress distribution during impact. Cross-ply laminates experienced higher stress due to load transfer in both longitudinal and transverse directions, whereas unidirectional laminates showed better load-carrying capability and lower stress concentrations. These findings reinforce the well-established principle that fibre orientation governs stiffness, energy absorption, and damage tolerance in composite structures.

Projectile shape was found to be a critical factor in determining the deformation magnitude and the initiation of failure. Flat and spherical projectiles generated larger spatial displacements, attributed to their larger contact surfaces, while conical projectiles produced more localized loading. These differences significantly influence the type and extent of damage, confirming that projectile geometry must be carefully considered when assessing impact resistance or designing components exposed to impact hazards.

Application of Hashin's fibre and matrix damage criteria revealed distinct failure modes across varying velocities. Fibre-related damage occurred selectively depending on projectile shape and velocity, whereas matrix damage especially compressive matrix failure appeared consistently across most impact conditions. This highlights that matrix material is more vulnerable to low-velocity impact, playing a key role in the onset of delamination and failure propagation, and must therefore be a major focus in designing impact-resistant CFRP laminates.

ACKNOWLEDGEMENT

The authors would like to acknowledge Universiti Teknologi MARA, Cawangan Pulau Pinang and the Ministry of Education, Malaysia for providing the grant under FRGS/1/2018/TK03/UITM/02/3.

AUTHORS CONTRIBUTION

M.H. Ismail: Conceptualization, Methodology, Writing Original Draft.
R. Othman: Supervision, Validation, Review & Editing.
M.R. Aziz: Formal analysis, Resources.

DECLARATION OF COMPETING OF INTEREST

The authors declare that they have no known competing financial interests or personal relationships that could have influenced the work reported in this paper.

REFERENCES

[1] R. Talreja and C. V. Singh, *Damage and failure of composite materials*. 2012. doi: 10.1017/CBO9781139016063.

[2] C. H. Hsueh, "Interfacial debonding and fibre pull-out stresses of fibre-reinforced composites," *Materials Science and Engineering A*, vol. 123, no. 1, 1990, doi: 10.1016/0921-5093(90)90203-F.

[3] C. H. Hsueh, "Elastic load transfer from partially embedded axially loaded fibre to matrix," *J Mater Sci Lett*, vol. 7, no. 5, 1988, doi: 10.1007/BF01730704.

[4] D. J. Bull, A. E. Scott, S. M. Spearing, and I. Sinclair, "The influence of toughening-particles in CFRPs on low velocity impact damage resistance performance," *Compos Part A Appl Sci Manuf*, vol. 58, 2014, doi: 10.1016/j.compositesa.2013.11.014.

[5] M. O. W. Richardson and M. J. Wisheart, "Review of low-velocity impact properties of composite materials," *Composites Part A: Applied Science and Manufacturing*, vol. 27, no. 12 PART A. 1996. doi: 10.1016/1359-835X(96)00074-7.

[6] S. H. Lee, H. Kim, S. Hang, and S. K. Cheong, "Interlaminar fracture toughness of composite laminates with CNT-enhanced nonwoven carbon tissue interleave," *Compos Sci Technol*, vol. 73, no. 1, 2012, doi: 10.1016/j.compscitech.2012.09.011.

[7] N. Odagiri, H. Kishi, and M. Yamashita, "Development of torayca prepreg p2302 carbon fibre reinforced plastic for aircraft primary structural materials," *Advanced Composite Materials*, vol. 5, no. 3, 1996, doi: 10.1163/156855196X00301.

[8] R. Othman, "Characterization of microscopic impact damage in CFRP laminates with toughened interlayers," Ehime University, 2017.

[9] S. W. Tsai and E. M. wu, "A General Theory of Strength for Anisotropic Materials," *J Compos Mater*, vol. 5, no. 1, 1971, doi: 10.1177/002199837100500106.

[10] K. Shigemori, A. Hosoi, Y. Fujita, and H. Kawada, "Fatigue strength properties of interlaminar toughened CFRP laminates under cyclic loading in the out-of-plane direction," *Transactions of the JSME (in Japanese)*, vol. 80, no. 812, 2014, doi: 10.1299/transjsme.2014smm0087

[11] P. P. Camanho, C. G. Dávila, and M. F. de Moura, "Numerical simulation of mixed-mode progressive delamination in composite materials," *J Compos Mater*, vol. 37, no. 16, 2003, doi: 10.1177/0021998303034505.

[12] *Abaqus Documentation*, 6.14. Dassault Systemes Simulia Corp.

[13] J. C. Brewer and P. A. Lagace, "Quadratic Stress Criterion for Initiation of Delamination," *J Compos Mater*, vol. 22, no. 12, 1988, doi: 10.1177/002199838802201205.

[14] M. L. Benzeggagh and M. Kenane, "Measurement of mixed-mode delamination fracture toughness of unidirectional glass/epoxy composites with mixed-mode bending apparatus," *Compos Sci Technol*, vol. 56, no. 4, 1996, doi: 10.1016/0266-3538(96)00005-X.

[15] T. Morimoto *et al.*, "JAXA advanced composites database," *jaxa research and development memorandum. Tech. Rep.; JAXA-RM-14-004*. 2015.

[16] M. Hojo, T. Ando, M. Tanaka, T. Adachi, S. Ochiai, and Y. Endo, "Modes I and II interlaminar fracture toughness and fatigue delamination of CF/epoxy laminates with self-same epoxy interleaf," *Int J Fatigue*, vol. 28, no. 10 SPEC. ISS., 2006, doi: 10.1016/j.ijfatigue.2006.02.004.

[17] K. Ogi, T. Tanaka, S. Yashiro, and A. Yoshimura, "High-velocity impact damage in CFRP unidirectional and cross-ply laminates," *Zairyo/Journal of the Society of Materials Science, Japan*, vol. 60, no. 5, 2011, doi: 10.2472/jsms.60.418.

[18] Yu, G., Ren, Y., Zhang, T., Xiao, W., & Jiang, H., "Hashin Failure Theory-Based Damage Assessment Methodology of Composite Tidal Turbine Blades," *China Ocean Engineering*, Vol. 32, pp. 216-225, 2018.

[19] G. Lu, T. Zhu, and Y. Xu, "Low velocity impact energy monitoring and recognition of composite laminates with variable thickness based on optical fibre sensor network," *Appl. Sci.*, vol. 11, no. 2, pp. 1–18, 2021, doi: 10.3390/app11020584.

[20] B. Magyar, T. Czigány, and G. Szebényi, "Metal-alike polymer composites: The effect of inter-layer content on the pseudo-ductile behaviour of carbon fibre/epoxy resin materials," *Composites Science and Technology*, vol. 215, p. 109002, 2021.

[21] S. A. Kumar and C. S. Lee, "A review of stress concentration studies on fibre composite laminates with holes and cut-outs," *Proc. Inst. Mech. Eng. Part L: J. Materials: Design and Applications*, vol. 234, no. 8, pp. 1177-1193, 2020.